

Effects of hydrotalcite intercalated with corrosion inhibitor on cathodic disbonding of epoxy coatings

To Thi Xuan Hang, Nguyen Thuy Duong, Trinh Anh Truc,
Thai Hoang, Dinh Thi Mai Thanh, Siriporn Daopiset,
Anothai Boonplean

© American Coatings Association 2015

Abstract In this study, zinc aluminum hydrotalcite intercalated with 2-benzothiazolythio-succinic acid (BTSA) as a container of corrosion inhibitor was prepared and incorporated in an epoxy coating. The HT-BTSA obtained was characterized using infrared spectroscopy and X-ray diffraction. BTSA release from HT-BTSA in 0.5 M NaCl solution was investigated using UV–Vis spectroscopy. The corrosion protection performance of the epoxy coating containing HT-BTSA was evaluated and compared to the pure epoxy coating and the epoxy coating containing HT by cathodic disbonding test, electrochemical impedance spectroscopy, salt spray test, and adhesion measurement. It was shown that the BTSA was intercalated in hydrotalcite and its loading was about 33.5%. The BTSA release from HT-BTSA increased with the pH of the NaCl solution. It was also shown that the presence of HT or HT-BTSA in epoxy coating improved the resistance to cathodic disbonding and the adhesion of the epoxy coating. Corrosion protection performance of epoxy coating containing HT-BTSA was higher than that of epoxy coating containing HT.

Keywords Epoxy coatings, Hydrotalcite, Corrosion inhibitors, Release, Cathodic disbonding, Corrosion protection

T. T. X. Hang (✉), N. T. Duong, T. A. Truc,
T. Hoang, D. T. M. Thanh
Institute for Tropical Technology, Vietnam Academy
of Science and Technology, 18 Hoang Quoc Viet,
Cau Giay, Hanoi, Vietnam
e-mail: tttxhang@itt.vast.vn

S. Daopiset, A. Boonplean
Thai-French Innovation Institute, King Mongkut's
University of Technology North Bangkok, 1518,
Pracharat 1 Rd., Bangsue, Bangkok 10800, Thailand

Introduction

Organic coatings are extensively used for corrosion protection of steel structures. Protection performance of organic coatings depends on the intrinsic properties of the organic film (barrier properties), adhesion of the coating, and the inhibitive efficiency of the corrosion inhibitors used. However, due to problems of high toxicity associated with inhibitive pigments such as strontium or zinc chromates, there are many studies on the development of more environmentally friendly organic coatings.

Hydrotalcites can be used to immobilize anionic inhibitors.^{1–4} The release of inhibitor anions can be triggered by the exchange with aggressive corrosive chloride ions. The anion-exchange pigments can play two roles: absorbing the harmful chlorides and releasing the inhibiting ions in response. The hydrotalcites containing decavanate and molybdate have been studied in organic coatings for corrosion protection of aluminum alloys. However, coatings containing ZnAl hydrotalcite intercalated with decavanate are not capable of protection equivalent to that of coatings containing chromate.

MgAl-HT and ZnAl-HT doped with divanate anions as a corrosion inhibitor were used in primers for corrosion protection of 2024 aluminum alloy. Electrochemical measurements and accelerated corrosion tests showed that coatings doped with ZnAl-HT provide better corrosion protection compared to that of chromate-based coatings.⁵

There are also studies on corrosion protection of aluminum alloy using coatings containing hydrotalcite-bearing organic anions such as benzotriazolates, ethyl xanthate, and oxalate.⁶ The results showed that inhibition efficiency depends on the structure of the organic anion and that inhibition efficiency increases in the order ethyl xanthate < oxalate < benzotriazolates. Benzotriazolates has been shown to interact specifically

with the alloy surface. Also, 2-benzothiazolythio-succinic acid (BTSA) is well known as an organic corrosion inhibitor used in organic coatings.⁷ It was observed that BTSA can be adsorbed on the iron oxide layers which are always present on steel surfaces and can form insoluble precipitates with ferrous ions.

In our previous studies, nanocontainers of corrosion inhibitor based on hydrotalcite were prepared.^{8,9} It was shown that the presence of BTSA-intercalated MgAl hydrotalcite improved the corrosion protection of epoxy coating. Additionally, modified ZnAl hydrotalcite provides higher corrosion inhibition of carbon steel than modified MgAl hydrotalcite.

This work investigates the effect of ZnAl hydrotalcite intercalated with BTSA on the cathodic disbonding of epoxy coating. The degradation of coatings due to cathodic disbonding was evaluated using electrochemical impedance spectroscopy. The steel surface under the coating after cathodic disbonding was analyzed by SEM and EDX. Corrosion protection performance of coatings was also evaluated by salt spray test and adhesion measurement.

Materials and methods

Materials

Sodium hydroxide, zinc nitrate hexahydrate, $\text{Zn}(\text{NO}_3)_2 \cdot 6\text{H}_2\text{O}$, and aluminum nitrate nonahydrate $\text{Al}(\text{NO}_3)_3 \cdot 9\text{H}_2\text{O}$ were purchased from Merck. Corrosion inhibitor, BTSA, was obtained from Ciba Company.

Preparation of hydrotalcite

The zinc aluminum hydrotalcite (HT) was synthesized using the co-precipitation method.¹⁰ The preparation was performed in a nitrogen atmosphere to exclude CO_2 which would lead to the incorporation of carbonate in the HT. A solution of 0.125 mol of $\text{Zn}(\text{NO}_3)_2 \cdot 6\text{H}_2\text{O}$ and 0.0625 mol of $\text{Al}(\text{NO}_3)_3 \cdot 9\text{H}_2\text{O}$ in 125 ml of degassed distilled water was added drop by drop over 1 h to a solution of 0.313 mol of NaOH in 145 ml of degassed distilled water. The pH of the solution was maintained at 8–10 by adding 1 M NaOH solution as needed. The resulting white precipitate was aged for 24 h at 65°C, and then filtered until all of the supernatant liquids were removed. The sample was washed several times with large amounts of degassed distilled water and dried at 50°C in a vacuum oven.

Preparation of hydrotalcite intercalated with BTSA

The zinc aluminum layered doubled hydroxides intercalated with BTSA (HT-BTSA) were prepared using the co-precipitation method.¹⁰ A solution of 0.125 mol of $\text{Zn}(\text{NO}_3)_2 \cdot 6\text{H}_2\text{O}$ and 0.0625 mol of $\text{Al}(\text{NO}_3)_3 \cdot 9\text{H}_2\text{O}$

in 125 ml of degassed distilled water was added to a dropwise solution of 0.313 mol of BTSA with the molar equivalent of NaOH in 145 ml of degassed distilled water with vigorous mixing under an inert nitrogen atmosphere. The pH of the solution was maintained at 8–9 by adding 1 M NaOH solution. The resultant slurry was aged at 65°C for 24 h, cooled to room temperature, and repeatedly washed with large amounts of degassed distilled water before drying at a temperature of 50°C for 24 h in a vacuum oven.

Preparation of epoxy coatings

Carbon steel sheets (150 mm × 100 mm × 2 mm) were used as substrates. The sheets were polished with abrasive papers from 80 to 600 grades and cleaned with ethanol.

The epoxy resin was epoxy bisphenol A, Epotec YD 011-X75; epoxy equivalent weight is about 469–490 g/eq. The hardener was modified polyamine. Both compounds were purchased from Thai Organic Chemicals Co. (Thailand). The hydrotalcites were incorporated in epoxy resin at 3 wt%. The hydrotalcites were dispersed with epoxy resin by magnetic stirring and then sonication. The liquid paint was applied by spin coating at 600 rpm for 1 min and dried at ambient temperature for 7 days. The dry film thickness was $30 \pm 3 \mu\text{m}$ (measured by Minitest 600 Erichen digital meter).

Analytical characterizations

The FTIR spectra of BTSA and synthesized HTs were obtained using the KBr method on a Nexus 670 Nicolet spectrometer operated at 1 cm^{-1} resolution in the 400–4000 cm^{-1} region.

Powder X-ray diffraction patterns of synthesized HTs were taken using a Siemens diffractometer D5000 with Cu K_α radiation (1.5406 Å) at room temperature under ambient air conditions.

The steel surface under coatings after cathodic disbonding was observed and analyzed by a LEO 1455VP spectrometer equipped with an EDAX microanalyser.

The loading amount of BTSA in HT-BTSA was determined using the following protocol: 0.05 g of HT-BTSA and 0.5 ml of 6 M HNO_3 solutions were mixed in a 10-ml volumetric flask, and the balance was filled with ethanol. The concentration of BTSA in the resulting solution was determined using UV–Vis spectroscopy at $\lambda_{\text{max}} = 283 \text{ nm}$.¹⁴ The concentration was calculated using a calibration curve obtained from a series of standard solutions of BTSA from 1×10^{-5} to $3 \times 10^{-4} \text{ M}$.

BTSA release from HT-BTSA

The BTSA release from HT-BTSA in 0.5 M NaCl solution at pH 7 and pH 10 was determined using the

following method: 0.5 g of HT-BTSA was dispersed in 500 ml of 0.5 M NaCl solution in water/ethanol under magnetic stirring. Aliquots (2 ml) of supernatant were withdrawn at different times and replaced with the same amount of fresh medium. The withdrawn aliquots were filtered, and their BTSA contents were determined by UV–Vis spectroscopy at 283 nm. Release experiments were performed in triplicate. UV–Vis spectra of solutions containing BTSA were obtained using a GBC CINTRA 40 spectrometer operated in the 200–400 nm regions.

Electrochemical characterization

For the electrochemical measurements, a three-electrode cell was used with a large platinum auxiliary electrode, a saturated calomel reference electrode (SCE), and a working electrode with an exposed area of 1.77 cm². For cathodic disbonding, the specimens were subjected to cathodic potential at -1500 mV/SCE for 24, 48, and 96 h. At the end of the specified periods, electrochemical impedance measurement was done on the corrosion potential on those specimens. The electrochemical impedance measurements were performed using a VMP3-BioLogic Science Instruments with seven points per decade using 30 mV peak-to-peak sinusoidal voltage. The corrosive medium was the 0.5 M NaCl solution. For each system, three samples were tested to ensure reproducibility.

Salt spray test

A salt spray test was performed according to ASTM B117 using a Q-FOGCT-600 chamber for 96 h, and at the end of the test, samples were evaluated according to ASTM D1654 and ASTM D714.^{11–13}

Adhesion measurement

The adhesion strength of the coatings was determined according to ASTM D4541 by a PosiTest digital pull-off adhesion tester (DeFelsko) with 20 mm dollies.¹⁴ The experiments involved pulling dollies affixed with a two-part Araldit epoxy adhesive away from the coated substrate. The maximum force by which the dolly lifts the coating from the steel plate was recorded as a measure of the bond strength between the coating and the substrate. The wet adhesion test was conducted after 48 h of immersion in 0.5 M NaCl solution.

Results and discussion

Characterization of HT-BTSA

BTSA loading of HT-BTSA was determined using UV–Vis spectroscopy. The calibration curve deter-

mined from a series of standard BTSA solutions was $C = 0.8518 A$, where C is the concentration of BTSA (in 10^{-4} mol/L) and A is the absorption intensity at 283 nm. The BTSA loading in HT-BTSA was 33.5%.

Fourier transformation infrared spectroscopy (FTIR) was used to confirm the presence of BTSA in the HT-BTSA. The FTIR spectra of BTSA, HT, and HT-BTSA are shown in Fig. 1.

The FTIR spectrum of HT shows strong peaks at 424, 1385, and 1631 cm⁻¹, characteristic of Zn–O vibrations, NO₃⁻ group, and water molecules in the interlayer domain.¹⁵

The spectrum of BTSA shows two bands at 3421 and 3062 cm⁻¹, characteristic of the OH and CH groups of aromatic ring structure. The band at 1721 cm⁻¹ is attributed to the vibration of group COOH. The band at 758 cm⁻¹ is attributed to the aromatic ring with four adjacent hydrogen atoms.¹⁶

The spectrum of HT-BTSA displays the bands characteristic of Zn–O vibrations of the hydroxide layer at 421 cm⁻¹. It is also observed that for HT-BTSA, the bands characteristic of the COOH group in the BTSA at 1721 cm⁻¹ disappeared and new bands at about 1586 and 1402 cm⁻¹ appeared. These bands can be assigned to asymmetric and symmetric vibrations of COO⁻ groups.¹⁶ The band characteristic of the aromatic ring with four adjacent hydrogen atoms also appears at 764 cm⁻¹ in the spectrum of HT-BTSA. This result revealed the existence of BTSA in the form of carboxylate in the interlayer of hydrotalcite.

The X-ray diffraction patterns of synthesized HT and HT-BTSA are shown in Fig. 2. The XRD pattern of the HT exhibits the (003) reflection, corresponding to the basal spacing of the hydroxide layer of 0.78 nm, which is close to the values reported in literature.¹⁷ In the XRD pattern of HT-BTSA, the value of the (003) reflection corresponds to the basal spacing of 1.73 and

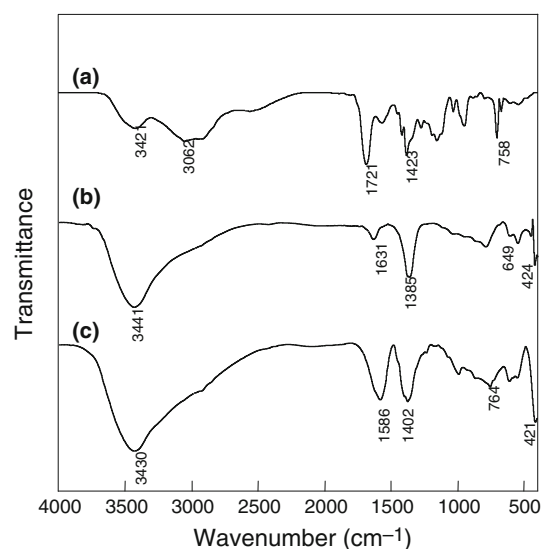


Fig. 1: FTIR spectra of (a) BTSA, (b) HT, and (c) HT-BTSA

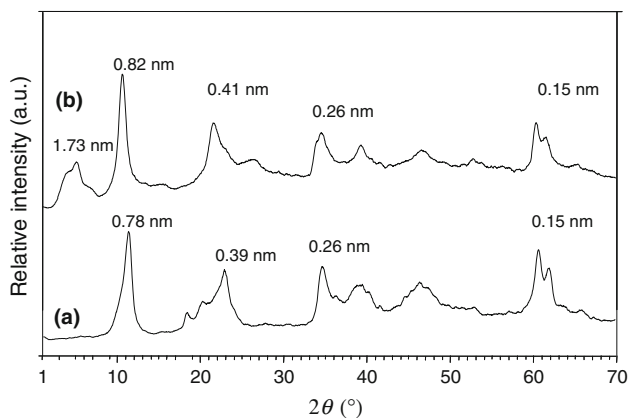


Fig. 2: XRD patterns of (a) HT and (b) HT-BTSA

0.82 nm. The higher d-spacing values of the HT-BTSA compared to that of HT show that BTSA was intercalated in the interlayer domain and replaced the NO_3^- anion.

Release of BTSA from HT-BTSA

The corrosion process generally occurs in the presence of an aggressive anion in the solution. The inhibitor release in the presence of an anion is expected to impede corrosion and confer self-healing properties to the organic coatings. The BTSA release from HT-BTSA was investigated in 0.5 M NaCl solution at pH 7 and 10. The release curves of BTSA from HT-BTSA are shown in Fig. 3. It was observed that for two solutions, there was a rapid release within the initial 8 h, followed by a slower release. This result is similar to that in the literature.¹⁸ The BTSA release in the solution at pH 10 was much higher than in the solution at pH 7. After 72 h of immersion in 0.5 M NaCl solution at pH 7 and pH 10, the BTSA release was 50.4% and 65.3%, respectively. The increase in BTSA release with the increase in solution pH can be attributed to the ion-exchange reaction of HT-BTSA with the OH^- anion.^{19,20}

Cathodic disbonding test

The impedance diagrams were plotted at the corrosion potential after different cathodic disbonding times to follow the degradation of coatings during exposure to cathodic disbondment. Figures 4 and 5 present the impedance diagrams of coatings before and after 48 h of cathodic disbonding. The electrochemical impedance diagram of an organic coating was interpreted as follows: the high-frequency part is related to the organic coating, while the low-frequency (LF) part corresponds to the reactions occurring on the metal through defects and pores in the coating.^{21,22}

At the initial state, the impedance diagrams of epoxy coating and epoxy coating containing 3 wt% HT are characterized by two time constants, while the

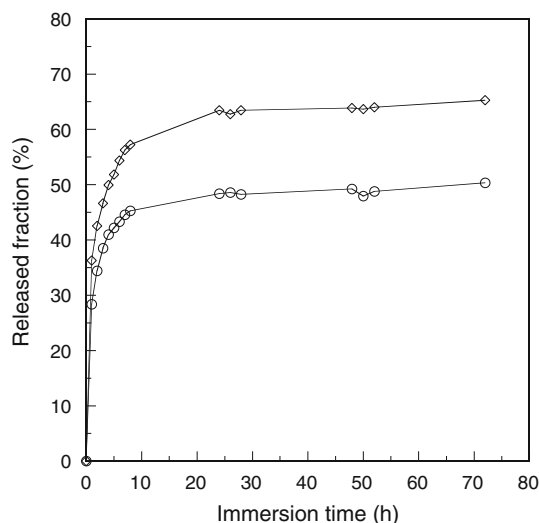


Fig. 3: Release curves of BTSA from HT-BTSA in (o) 0.5 M NaCl solution at pH 7 and (◇) 0.5 M NaCl solution at pH 10

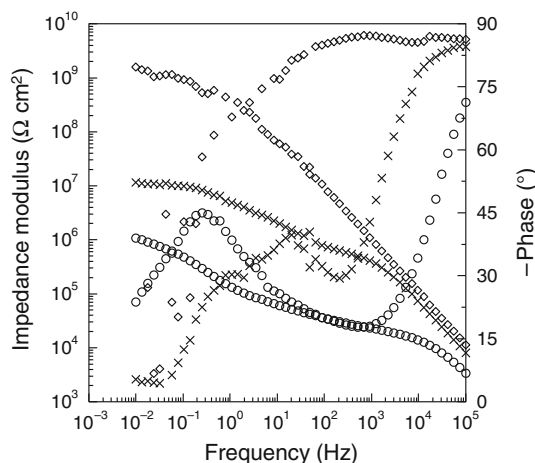


Fig. 4: Electrochemical impedance diagrams obtained before exposure to cathodic disbonding for carbon steel covered by (o) epoxy coating, (x) epoxy coating containing 3 wt% HT, and (◇) epoxy coating containing 3 wt% HT-BTSA

impedance diagram of epoxy coating containing 3 wt% HT-BTSA presents a single time constant. The impedance modulus of epoxy coating containing 3 wt% HT is higher than that of pure epoxy coating. The highest impedance modulus is observed for epoxy coating containing 3 wt% HT-BTSA. This system displays capacitive behavior with very high impedance modulus at low frequencies ($>10^9 \Omega \text{ cm}^2$) with a phase angle close to -90° for most of the frequency range.

The improvement of the barrier properties of coatings by the presence of HT and HT-BTSA can be explained by the increase in the tortuous diffusion pathway of oxygen and water, and trapping of Cl^- ions by hydrotalcite dispersed in the epoxy matrix.^{23,24} The

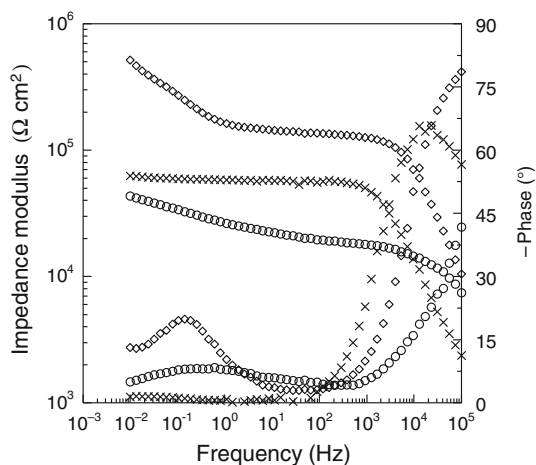


Fig. 5: Electrochemical impedance diagrams obtained after 48 h exposure to cathodic disbonding for carbon steel covered by (o) epoxy coating, (x) epoxy coating containing 3 wt% HT, and (◇) epoxy coating containing 3 wt% HT-BTSA

higher impedance modulus obtained with HT-BTSA by comparison with HT can be explained by better dispersion in the epoxy matrix due to the organic modification by BTSA.

After 48 h exposure to cathodic disbonding, the impedance modulus of all coatings decreased. The decrease in impedance modulus indicates the degradation of coatings under cathodic disbonding. The cathodic disbonding caused the migration of water and oxygen and Na^+ ions, necessary in order to locally balance the electric charge, through the coatings to the interface coating/steel.^{25,26}

The impedance modulus at low frequencies of coatings containing hydrotalcites was higher than that of pure epoxy coating. The impedance modulus of epoxy coating containing 3 wt% HT-BTSA was much higher than that of epoxy coating containing 3 wt% HT. This result indicates that the epoxy coating containing 3 wt% HT-BTSA is the most resistant to cathodic disbondment.

The higher impedance modulus at low frequencies obtained with hydrotalcites can be explained by the improvement of the barrier properties and adhesion of epoxy coatings by the presence of hydrotalcites. The higher impedance modulus obtained with HT-BTSA by comparison with HT can be explained by higher barrier properties and the role of BTSA released at the interface coating/steel. The reaction of BTSA released with the steel surface reduced the cathodic reaction.⁷

It was proposed by Kittel et al.²⁷ and the group of Bierwagen^{28–30} that the impedance modulus at low frequencies measured vs exposure time could serve as an estimation of the corrosion protection of a painted metal. Figure 6 plots $|Z|_{105\text{mHz}}$ vs cathodic disbonding time for the carbon steel covered by pure epoxy coating, epoxy coating containing 3 wt% HT, and epoxy containing 3 wt% HT-BTSA. For all coatings,

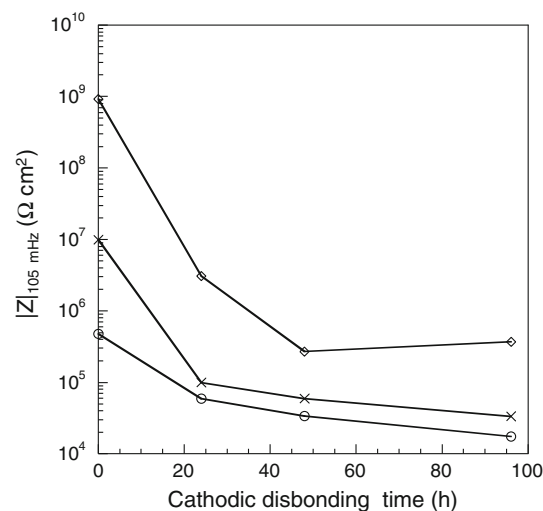


Fig. 6: $|Z|_{105\text{ mHz}}$ vs cathodic disbonding time for the carbon steel covered by (o) epoxy coating, (x) epoxy coating containing 3 wt% HT, and (◇) epoxy coating containing 3 wt% HT-BTSA

the $|Z|_{105\text{mHz}}$ values decreased rapidly during the first 48 h of testing. This result indicates a rapid loss of the protective properties of the film due to the cathodic disbondment. After this exposure time, the $|Z|_{105\text{mHz}}$ values continued to decrease for the pure epoxy coating and epoxy coating containing 3 wt% HT. For the epoxy coating containing 3 wt% HT-BTSA, the $|Z|_{105\text{mHz}}$ values remained relatively stable at high value. After 96 h exposure to cathodic disbonding, the $|Z|_{105\text{mHz}}$ value of epoxy coating containing 3 wt% HT-BTSA was much higher than that of pure epoxy coating and epoxy coating containing 3 wt% HT. The $|Z|_{105\text{mHz}}$ value of epoxy coating containing 3 wt% HT was higher than the $|Z|_{105\text{mHz}}$ value of the pure epoxy coating. The considerably higher $|Z|_{105\text{mHz}}$ value was obtained using the presence of HT-BTSA in comparison with the one obtained from the presence of HT, which can be explained by the reaction of BTSA released from HT-BTSA at the steel surface.⁷ BTSA can be released from HT-BTSA by the exchange reaction with anions like Cl^- and OH^- . BTSA released can be adsorbed onto the iron oxide layers and form insoluble precipitates with ferrous ions, so that it can reduce the cathodic reaction. These results show that the addition of HT-BTSA significantly improved the resistance of epoxy coating to cathodic disbonding.

Photographs of coating surfaces after 96 h of cathodic disbonding are presented in Fig. 7. For pure epoxy coating, blistering and cracks in the coating are observed. For epoxy coating containing 3 wt% HT, we also see blistering of the coating. For epoxy coating containing 3% HT-BTSA, no blister is observed. These results indicate that epoxy coating containing 3% HT-BTSA displays the highest resistance to cathodic disbonding. This observation agrees with the results obtained by impedance measurements.

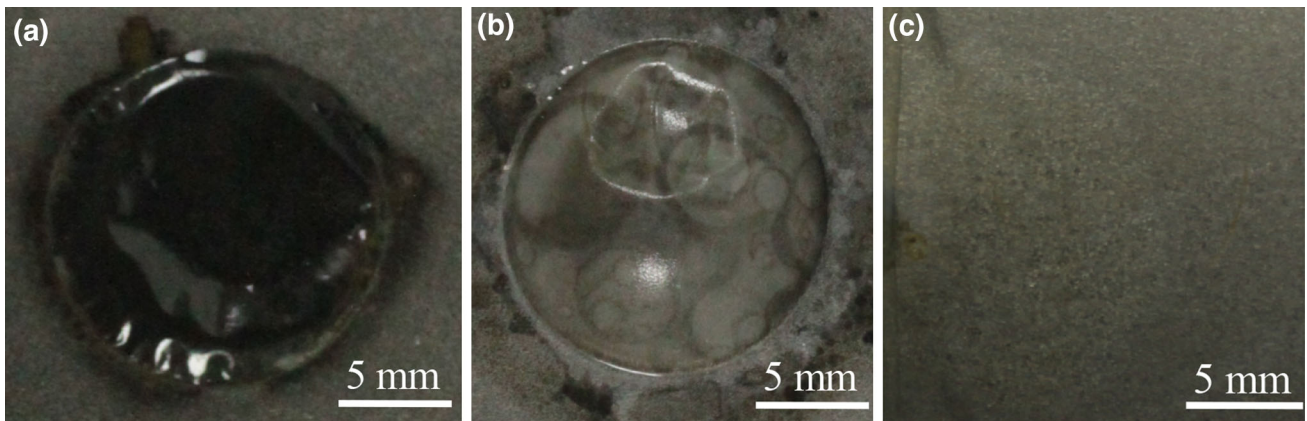


Fig. 7: Photographs of samples after 96 h exposure to cathodic disbonding for carbon steel covered by (a) epoxy coating, (b) epoxy coating containing 3 wt% HT, and (c) epoxy coating containing 3 wt% HT-BTSA

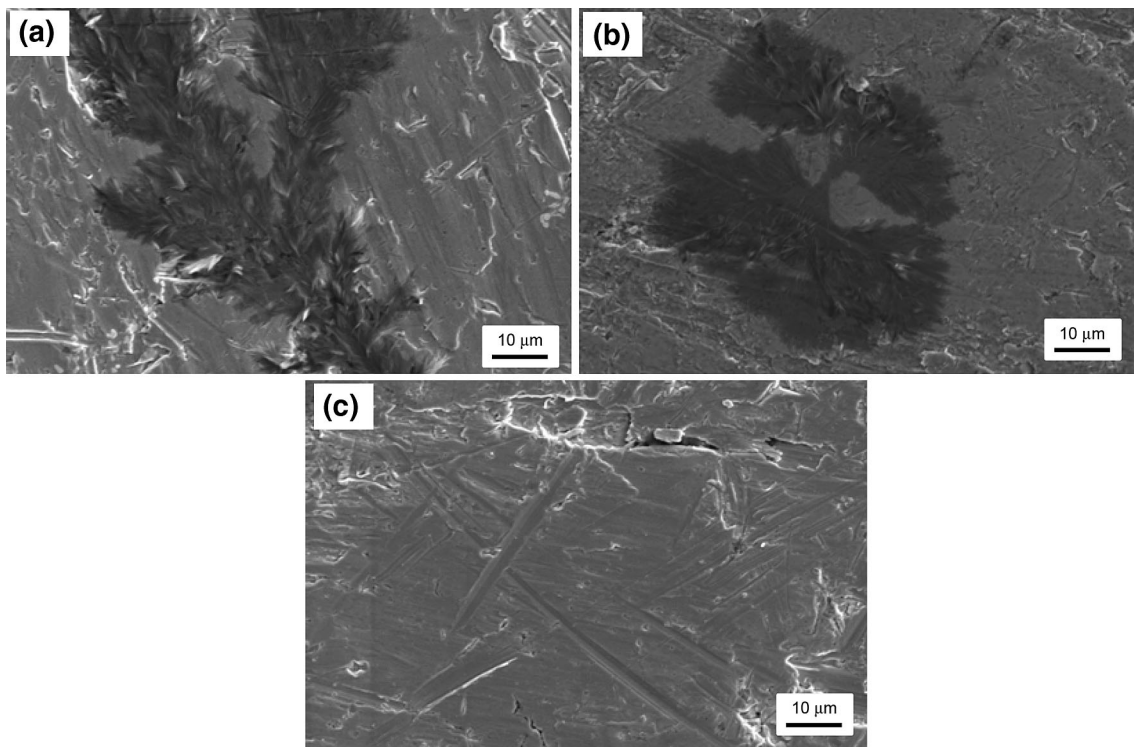


Fig. 8: SEM photographs after 96 h exposure to cathodic disbonding of steel surface under (a) epoxy coating, (b) epoxy coating containing 3 wt% HT, and (c) epoxy coating containing 3 wt% HT-BTSA

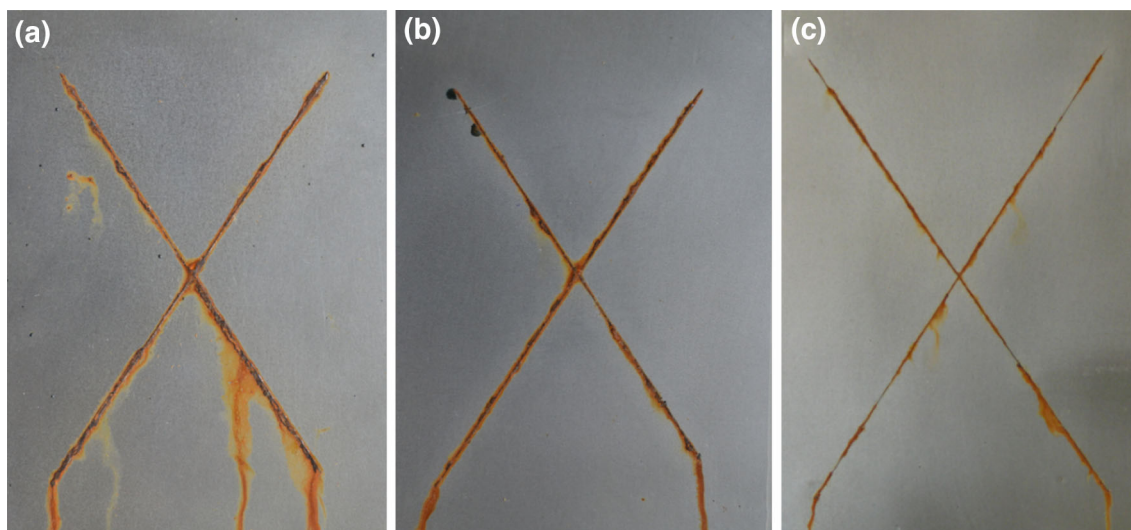
SEM photographs of the steel surface under coatings after 96 h exposure to cathodic disbonding are shown in Fig. 8, and the element analysis by EDX is presented in Table 1. For three coatings, different morphologies at the steel surface are observed. For pure epoxy coating and epoxy coating containing 3 wt% HT, crystals of iron oxide are observed. In the case of epoxy coating containing HT-BTSA, only very small crystals of iron oxide are observed. The quantity of iron oxide formed

at the steel surface was considerably lower compared to the steel surface under pure epoxy coating and epoxy coating containing 3 wt% HT.

The EDX analysis of the steel surface under coatings shows high oxygen content in the cases of pure epoxy coating and epoxy coating containing 3 wt% HT and low oxygen content for epoxy coating containing 3 wt% HT-BTSA. Besides that, for pure epoxy coating and epoxy coating containing 3 wt% HT, it observed

Table 1: EDX elemental analysis of steel surface under coatings after 96 h exposure to cathodic disbonding

Samples	O		Fe		S		Na	
	(wt%)	(at.%)	(wt%)	(at.%)	(wt%)	(at.%)	(wt%)	(at.%)
Epoxy coating	32.65	49.60	33.44	14.56	0	0	33.91	35.85
Epoxy coating containing 3 wt% HT	34.18	52.25	35.58	15.58	0	0	30.24	32.17
Epoxy coating containing 3 wt% HT-BTSA	9.65	27.07	89.8	72.16	0.55	0.77	0	0

**Fig. 9: Photographs of samples after 96 h exposure to salt spray testing of (a) epoxy coating, (b) epoxy coating containing 3% HT, and (c) epoxy coating containing 3% HT-BTSA**

the presence of Na at the steel surface under coatings. These results indicate that more iron oxide formed under the coating in the case of pure epoxy coating and epoxy coating containing 3 wt% HT and less iron oxide formed under the coating for epoxy coating containing 3 wt% HT-BTSA. For pure epoxy coating and epoxy coating containing 3 wt% HT, the Na⁺ ions diffused through the coatings toward the interface and introduced the delamination of coatings, but this was not observed for epoxy coating containing 3 wt% HT-BTSA. The delamination degrees of pure epoxy coating and epoxy coating containing 3 wt% HT were higher than that of epoxy coating containing 3 wt% HT-BTSA. The SEM and EDX analysis results are in good agreement with the impedance measurements.

Salt spray test

The salt spray test was conducted as an accelerated corrosion test to evaluate the corrosion resistance of carbon steel covered with pure epoxy, epoxy containing 3 wt% HT, and epoxy coating containing 3 wt% HT-BTSA. The photographs of samples after 96 h exposure to salt spray test are shown in Fig. 9. The evaluation of the corrosion behavior of coatings

according to ASTM D1654 and ASTM D714 is presented in Table 2. For epoxy coating, the brown rusty corrosion products accumulated on the scratches increased and there was some corrosion and numerous blisters on the surface. For epoxy coating containing 3% HT, at the scratches, it is observed that some blisters and corrosion products were formed but the corrosion degree is lower in comparison to pure epoxy coating. For epoxy coating containing 3 wt% HT-BTSA, no blister was found and the corrosion products formed at scratches were limited. The rust creepage from scribe of the pure epoxy was higher coating than that of epoxy containing hydrotalcite. According to ASTM D1654, the rating numbers were 8 for pure epoxy coating and 9 for epoxy coating containing HT and HT-BTSA after 96 h of exposure to the salt spray test.

The salt spray test results indicate that the presence of HT and HT-BTSA improved the corrosion resistance of epoxy coating, and the HT-BTSA provided higher protection. These results indicate the inhibitory action of BTSA at the coating/metal interface. The salt spray test results are in good agreement with the cathodic disbonding test which indicates that the presence of HT-BTSA significantly improved the corrosion protection performance of epoxy coating.

Table 2: Salt fog test results according to ASTM D1654 and ASTM D714 standards

Samples	Creepage from scribe		Blistering degree
	Rust creepage (mm)	Rating number	
Epoxy coating	0.76	8	8F
Epoxy coating containing 3 wt% HT	0.49	9	10
Epoxy coating containing 3 wt% HT-BTSA	0.26	9	10

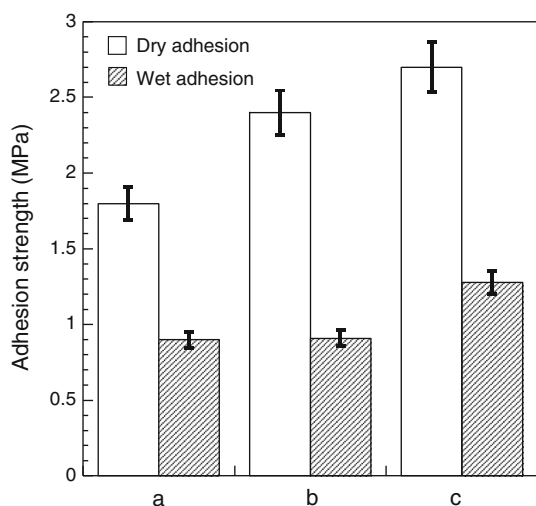


Fig. 10: Pull-off adhesion strength in wet and dry states of (a) epoxy coating, (b) epoxy coating containing 3 wt% HT, and (c) epoxy coating containing 3 wt% HT-BTSA

Adhesion measurements

The corrosive electrolyte diffusion into the coating/metal interface causes a decrease in the adhesion of the coating on the metal substrate. The wet and dry pulls of adhesion strength of coatings are shown in Fig. 10. It is shown that the dry adhesion of epoxy coating containing 3 wt% HT-BTSA is much higher than that of pure epoxy coating and epoxy coating containing 3 wt% HT. For all coatings, the wet adhesion is lower than dry adhesion. However, the wet adhesion of epoxy coating containing HT-BTSA is considerably higher than that of pure epoxy coating and epoxy coating containing 3 wt% HT. The increase in coating adhesion with the presence of HT-BTSA can be explained by the interaction of BTSA with the steel surface. These adhesion results are in good agreement with the salt spray test and cathodic disbonding test.

Conclusions

Zinc aluminum hydrotalcite intercalated with BTSA was successfully synthesized using the co-precipitation method. The BTSA release from HT-BTSA was investigated in a 0.5 M NaCl solution with different

pHs. The BTSA release from HT-BTSA was superior to the higher solution pH. After 72 h of immersion in 0.5 M NaCl solution at pH 10, 65.3% of BTSA was released from HT-BTSA. The impedance measurement and surface analysis showed that the presence of HT-BTSA significantly enhanced the resistance to cathodic disbonding of the epoxy coating. From the salt spray test and adhesion measurement, it was found that the addition of HT-BTSA improved corrosion resistance and adhesion of the epoxy coating. The corrosion protection performance of epoxy coating containing HT-BTSA was explained by the corrosion inhibition at the steel surface due to BTSA released from HT-BTSA.

Acknowledgments This research was funded by the Vietnam National Foundation for Science and Technology Development (NAFOSTED) under Grant number 104.01-2012.15. The authors gratefully acknowledge the support of Vietnam Academy of Science and Technology and Thai-French Innovation Institute.

References

- Leggat, RB, Zhang, W, Buchheit, RG, Taylor, SR, "Performance of Hydrotalcite Conversion Treatments on AA2024-T3 When Used Within a Coating System." *Corrosion*, **58** 322–328 (2002)
- Wang, H, Presuel, F, Kelly, RG, "Computational Modeling of Inhibitor Release and Transport from Multifunctional Organic Coatings." *Electrochim. Acta*, **49** 239–255 (2004)
- Buchheit, RG, Guan, H, Mahajanam, S, Wong, F, "Active Corrosion Protection and Corrosion Sensing in Chromate-Free Organic Coatings." *Prog. Org. Coat.*, **47** 174–182 (2003)
- Mahajanam, PV, Buchheit, RG, "Characterization of Inhibitor Release from Zn-Al-[V10O28]⁶⁻ Hydrotalcite Pigments and Corrosion Protection from Hydrotalcite-Pigmented Epoxy Coatings." *Corrosion*, **64** 230–240 (2008)
- Zheludkevich, ML, Poznyak, SK, Rodrigues, LM, Raps, D, Hack, T, Dick, LF, Nunes, T, Ferreira, MGS, "Active Protection Coatings with Layered Double Hydroxide Nancontainers of Corrosion Inhibitor." *Corros. Sci.*, **52** 602–611 (2010)
- Williams, G, McMurray, HN, "Inhibition of Filiform Corrosion on Polymer Coated AA2024-T3 by Hydrotalcite-Like Pigments Incorporating Organic Anions." *Electrochem. Solid-State Lett.*, **7** B13–B15 (2004)
- Braig, A, "Advances in corrosion protection by organic coatings." In: Sekine, I. (ed.) *Electrochemical Society. Corrosion Division*, pp. 18–30. (1998)

8. Hang, TTX, Truc, TA, Duong, NT, Pébère, N, Olivier, MG, “Layered Double Hydroxides as Containers of Inhibitors in Organic Coatings for Corrosion Protection of Carbon Steel.” *Prog. Org. Coat.*, **74** 343–348 (2012)
9. Hang, TTX, Truc, TA, Duong, NT, Vu, PG, Hoang, T, “Preparation and Characterization of Nanocontainers of Corrosion Inhibitor Based on Layered Double Hydroxides.” *Appl. Clay Sci.*, **67** 18–25 (2012)
10. Nyambo, C, Chen, D, Su, S, Wilkie, CA, “Variation of Benzyl Anions in MgAl-Layered Double Hydroxides: Fire and Thermal Properties in PMMA.” *Polym. Degrad. Stab.*, **94** 496–505 (2009)
11. ASTM B 117-09, *Standard Practice for Operating Salt Spray (Fog) Apparatus*. ASTM, Philadelphia, 2009
12. ASTM D1654, *Standard Test Method for Evaluation of Painted or Coated Specimens Subjected to Corrosive Environments*. ASTM, Philadelphia, 2008
13. ASTM D714, *Evaluating Degree of Blistering of Paints*. ASTM, Philadelphia, 1987
14. ASTM D4541-02, *Standard Test Method for Pull-Off Strength of Coatings Using Portable Adhesion Testers*. ASTM, Philadelphia, 2002
15. Xu, ZP, Braterman, PS, “Synthesis, Structure and Morphology of Organic Layered Double Hydroxide (LDH) Hybrids: Comparison Between Aliphatic Anions and Their Oxygenated Analogs.” *Appl. Clay Sci.*, **48** 235–242 (2010)
16. Simons, WW, *The Sadtler Handbook of Infrared Spectra*. Sadtler Research Laboratories Inc, Pennsylvania, 1978
17. Buchheit, RG, Guan, H, Mahajanam, S, Wong, F, “Active Corrosion Protection and Corrosion Sensing in Chromate-Free Organic Coatings.” *Prog. Org. Coat.*, **47** 174–182 (2003)
18. Qiu, DP, Hou, WG, “Synthesis and Characterization of Indole-3-Butyric Acid/Hydrotalcite-Like Compound Nanohybrids.” *Colloids Surf. A: Physicochem. Eng. Aspects*, **336** 12–17 (2009)
19. Hussein, MZB, Zainal, Z, Yahaya, AH, Foo, DWV, “Controlled Release of a Plant Growth Regulator, α -Naphthaleneacetate from the Lamella of Zn–Al-Layered Double Hydroxide Nanocomposite.” *J. Controll. Rel.*, **82** 417–427 (2002)
20. Radha, AV, Kamath, PV, Shivakumara, C, “Mechanism of the Anion Exchange Reactions of the Layered Double Hydroxides (LDHs) of Ca and Mg with Al.” *Solid State Sci.*, **7** 1180–1187 (2005)
21. Beaunier, L, Epelboin, I, Lestrade, JC, Takenouti, H, “Electrochemical and Scanning Microscope Study of Painted Fe.” *Surf. Technol.*, **4** 237–254 (1976)
22. Pébère, N, Picaud, T, Duprat, M, Dabosi, F, “Evaluation of Corrosion Performance of Coated Steel by the Impedance Technique.” *Corros. Sci.*, **29** 1073–1086 (1989)
23. Williams, G, McMurray, HN, “Anion-Exchange Inhibition of Filiform Corrosion on Organic Coated AA2024-T3 Aluminum Alloy by Hydrotalcite-Like Pigments.” *Electrochim. Solid-State Lett.*, **6** B9–B11 (2003)
24. Tedim, J, Kuznetsova, A, Salak, AN, Montemor, F, Snihirova, D, Pilz, M, Zheludkevich, ML, Ferreira, MGS, “Zn–Al Layered Double Hydroxides as Chloride Nanotraps in Active Protective Coatings.” *Corros. Sci.*, **55** 1–4 (2012)
25. Deflorian, F, Rossi, S, “An EIS Study of Ion Diffusion Through Organic Coatings.” *Electrochim. Acta*, **51** 1736–1744 (2006)
26. Leng, A, Streckel, H, Stratmann, M, “The Delamination of Polymeric Coatings from Steel. Part 1: Calibration of the Kelvin Probe and Basic Delamination Mechanism.” *Corros. Sci.*, **41** 547–578 (1999)
27. Kittel, J, Celati, N, Keddani, M, Takenouti, H, “Influence of the Coating–Substrate Interactions on the Corrosion Protection: Characterisation by Impedance Spectroscopy of the Inner and Outer Parts of a Coating.” *Prog. Org. Coat.*, **46** 135–147 (2003)
28. Bierwagen, GP, Tallman, D, Li, J, He, L, Jeffcoate, C, “EIS Studies of Coated Metals in Accelerated Exposure.” *Prog. Org. Coat.*, **46** 148–158 (2003)
29. De Rosa, RL, Earl, DA, Bierwagen, GP, “Statistical Evaluation of EIS and ENM Data Collected for Monitoring Corrosion Barrier Properties of Organic Coatings on Al-2024-T3.” *Corros. Sci.*, **44** 1607–1620 (2002)
30. Hinderliter, BR, Croll, SG, Tallman, DE, Su, Q, Bierwagen, GP, “Interpretation of EIS Data from Accelerated Exposure of Coated Metals Based on Modeling of Coating Physical Properties.” *Electrochim. Acta*, **51** 4505–4515 (2006)